Electronic Research Archive

ERA, 31(2): 776–792.
DOI: 10.3934/era.2023039
Received: 30 September 2022
Revised: 03 November 2022
Accepted: 14 November 2022
Published: 28 November 2022

http://www.aimspress.com/journal/ERA

Research article

Inversion study of vehicle frontal collision and front bumper collision

Miao Luo[1], Yousong Chen[1], Dawei Gao[2,*] and Lijun Wang[1]

[1] SAIC MOTOR Commercial Vehicle Technical Center, Shanghai 200483, China
[2] School of Mechanical Engineering, University of Shanghai for Science and Technology, Shanghai 200093, China

* **Correspondence:** Email: gddwww1999@163.com; Tel: +8613651844119.

Abstract: The collision of a vehicle is often a process of strong nonlinearity and large deformation, and the finite element method is time-consuming. For this reason, a method of collision inversion research is proposed. Through the definition of the forward and inverse problems, the forward problem is inversely solved from the perspective of the inverse problem, and the collision process can be predicted quickly while the accuracy is ensured. In this paper, the idea of inversion is introduced into the collision test of the front bumper of the vehicle. First, a finite element model is established based on the geometric model of the bumper. The accuracy of the finite element model is verified by comparing the results of the drop weight test with the simulation results of the finite element model. Then, using the built simulation model, spring mass model and drop weight test, the inversion research of vehicle collision and the front bumper of a vehicle is carried out. The inversion research of the bumper first inverts the collision course in the inversion algorithm derived from the vehicle collision, and then compares the collision course derived from the inversion algorithm formula with the simulation test results. The research results show that the change trends of the time-velocity curve and the time-deformation curve obtained by the collision inversion algorithm are basically consistent with the simulation test results, indicating that the collision inversion algorithm can realize the rapid prediction of the collision course and improve derivation efficiency significantly, and it provides a new idea. Finally, under the constant energy condition of the drop weight test E = mgh, through the relationship between energy and deformation, it is concluded that the depth deformation of low-speed collision of the front bumper is greater than that of high-speed collision.

Keywords: vehicle collision; front bumper; inversion study; collision course; low speed collision and high collision

1. Introduction

Research shows that among all accidents, front crash accidents cause the highest death toll, followed by side crashes [1]. In a front crash, the vehicle mainly depends on the bumper to absorb energy, especially in a low-speed front crash, where the energy-absorbing and anti-collision module of the bumper system can absorb a majority of the energy, therefore minimizing the damage to the vehicle body caused by the crash. A vehicle crash is a rather complicated strongly nonlinear process, and to simulate such a collision course, we need fine modeling to improve the computation accuracy, which will increase computation time and workload significantly [2]. For this reason, a collision inversion study method is proposed to realize fast prediction over the collision course. In addition, general vehicle crash problems are solved applying the forward problem analysis method based on a surrogate model, but this method is infeasible for some problems. Through the definition of the inverse problem, we can conduct inversion to solve the forward problem from the perspective of the inverse problem [3–8].

Backus and Gilbert first proposed the modern inversion method [9–11], which was initially studied in the field of ships. Zhang et al. [3] inverted the collision angle and collision speed of the ship through the results after the collision, which is very meaningful for the actual collision restoration. In the inversion research of the automotive industry, Han [6] studied the inversion problem of sheet metal forming, studied the types of inversion problems and introduced the engineering application of inversion in a very comprehensive manner. Aiming at the problem of lane keeping in autonomous driving, Yang et al. [8] proposed a kind of lateral position error composite control method that combines inversion control and sliding mode control. This method can retain the strong robustness of sliding mode control in uncertain lateral dynamic models. Gao [12] studied the key technologies of contact collision simulation through inversion. There are two main inversion methods: One is empirical inversion, where inversion is conducted through summarization of a large quantity of data; the other is theoretical inversion, where inversion is conducted through derivation of theoretical formulas. This study needs to use both.

Depending on the systemically mastered domestic and foreign vehicle crash inversion techniques, this study established a mass-spring simplified model and in turn used the simplified model derivation formulas for an inverse collision course. After a vehicle model is built, front collisions at various speeds are conducted. A nonlinear relationship between the energy absorption ratio of the automobile front bumper system and boundary conditions is fit through discrete change points of the boundary conditions. Finally, it is introduced into the crash test of a vehicle front bumper, and the deformation mode and energy absorption behavior of the front bumper are studied using a drop test. The conclusion is that the deformation of the front bumper in low-speed collision is larger than that in high-speed collision under the condition of equal energy.

2. Establishment and validation of finite element model

2.1. Establishment of finite element model (FEM)

This study conducted 3D modeling using CATIA, established the FEM using Altair Hypermesh and found and computed the solution using LS-DYNA. The original model of the bumper is the same as that of the vehicle. First of all, a 100% barrier vehicle collision FEM is built in accordance with vehicle crash high-

speed regulation C-NCAP. As shown in Figure 1, the forward direction of the vehicle is along the positive direction of the x-axis, hitting the rigid wall, and a rigid wall is also established at the bottom of the vehicle.

The bumper finite element model uses aluminum material. Considering that some elements need bear strong stress during the collision, which exceeds yield stress. The bumper belongs to the thin shell part, should draw the shell element, select the material model MAT_024. The bumper model has 21,693 elements, and the grid size is mainly 5 mm. The structural composition and size of the bumper are shown in Table 1, and the simulation model is shown in Figure 2.

Table 1. Initial bumper dimensions.

Device	Length /mm	Width /mm	Height /mm	Initial thickness /mm
Beam	1130	35	100	2.4
Energy-absorbing box	130	75	105	1.8
Flange	14	130	170	3.0

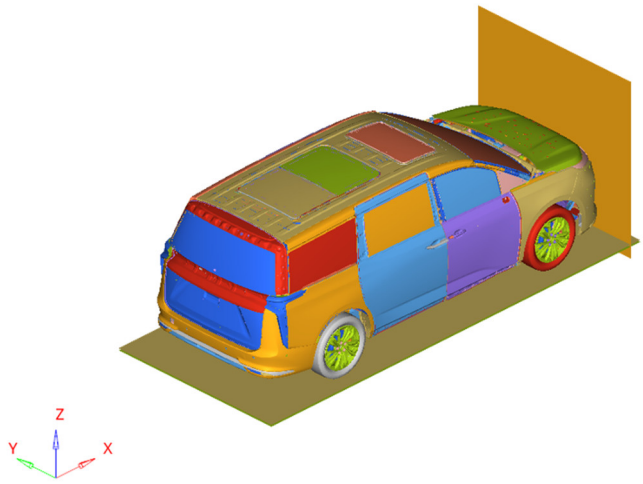

Figure 1. FEM of vehicle.

Figure 2. Simulative model of bumper.

Figure 3 shows the simulation timing diagram of the vehicle collision. During the collision, we can see that the vehicle front tends to descend, the front part of the bumper is crushed, and the maximum deformation position is close to the front part of the tire.

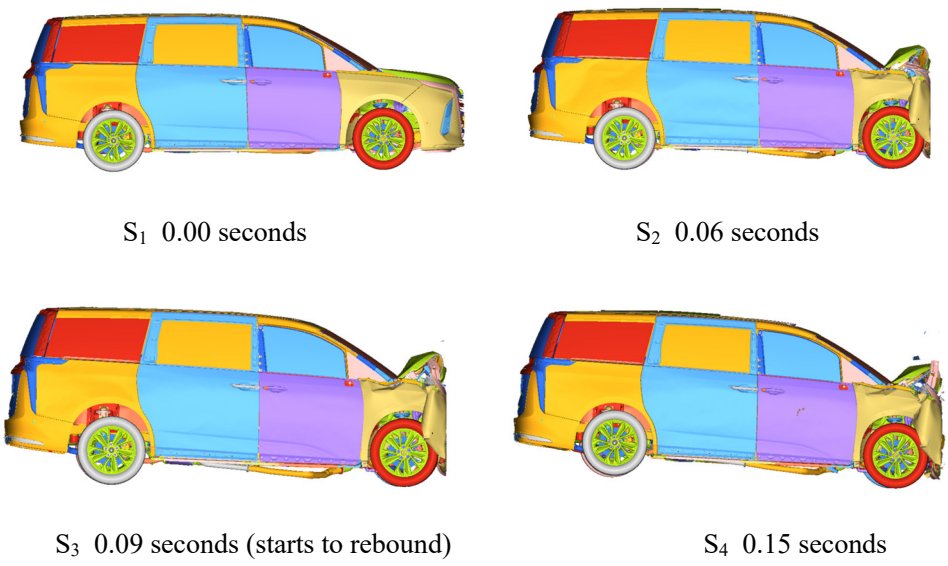

Figure 3. Simulation timing diagram of vehicle collision.

Figure 4 shows the solution-finding energy curve for the front crash. The blue line represents the curve of change in total energy during the crash. It can be seen from the figure that the total energy curve tends to be stable, and there is no major change, indicating that the total energy in the collision process satisfies the law of energy conservation. As the crash goes ahead, the kinetic curve descends dramatically before running levelly; in this process, kinetic energy is mainly converted into internal energy. The results of calculations based on the hourglass energy curve data shown in the figure show that hourglass energy contributes a maximum of 2.65% of total energy, which has no great impact on the calculation results, therefore meeting the requirement of the analysis for hourglass. The data obtained in the simulation will be used for the crash inversion computation, described in the section below.

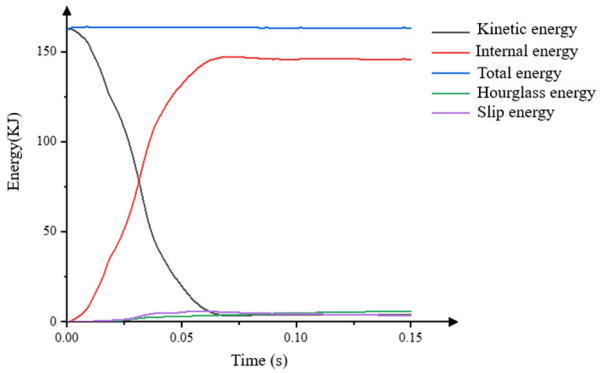

Figure 4. Solution-finding energy curve for vehicle front crash at 50 km/h.

2.2. Validation of bumper collision FEM

We compared the simulation and test to validate the built bumper FEM. The verification was made in two respects: first, captured collision altitude with high-speed camera; second, measured deformation

distance using laser rangefinder. According to the energy equivalent test method, the mass of the drop weight was 16.8 kg, the height of the drop weight was 2.128 m. The drop speed was 23.25 km/h.

Figure 5 shows the timing comparison diagram of FEM validation through experiment, in which the stress nephogram is shown for FEM. As shown in Figure 6, while the final deformation distance of FEM was 67.2 mm, the deformation distance measured in the test was 68 mm. They have 98.82% similarity to each other, so FEM proves effective.

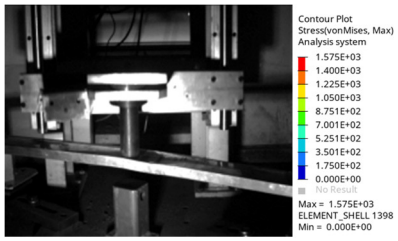

(a) Altitude and simulation stress of anti-collision beam at 0.001 s

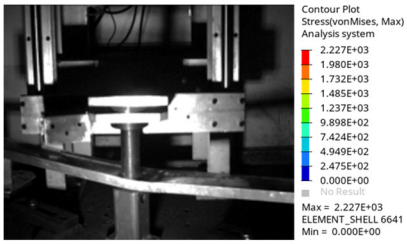

(b) Altitude and simulation stress of anti-collision beam at 0.01 s

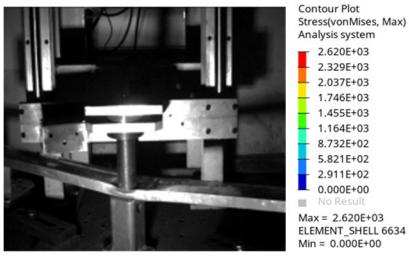

(c) Altitude and simulation stress of anti-collision beam at 0.025 s

Figure 5. Timing comparison of stress validation through experiments.

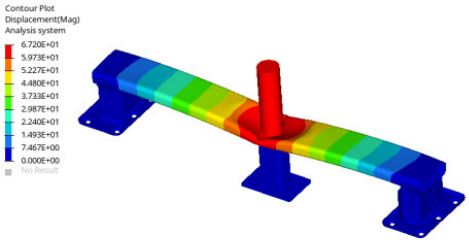

Figure 6. Final deformation and displacement nephogram of FEM.

3. Inversion analysis

3.1. Vehicle front crash inversion analysis

Inversion is conducted through theoretical formula deviation in vehicle front crash analysis, to complete the analysis of the vehicle front crash course. The study of frontal collision must first start with kinematics, and kinematics is inseparable from the acceleration and displacement of the basic vehicle collision. There are two kinds of curves in focus: One is the GS curve (the relationship between acceleration and displacement), and the other is the ES curve (the relationship between energy and displacement). The area enclosed by the GS curve and the X-axis is a fixed value [mv]_0^2/2; see [13] for the specific derivation. The ES curve has an obvious inflection point. The inflection point is the stage where the vehicle rebounds after a collision. The value of the ordinate is [mv]_0^2/2. The lower the collision speed is, the sharper the inflection point. In addition, the collision deceleration curve can also be replaced by the Tipped Equivalent Square Wave [14], especially in the acceleration curve of the occupant.

The 100% overlap rigid barrier crash test is a very good test method for the study of crashworthiness features of vehicles. Under NCAP, the high-speed collision velocity of the 100% overlap rigid barrier crash test is 50 km/h. The impact force (F) that the rigid barrier exerts on the vehicle is very strong and very brief. For this reason, the force on the vehicle other than the impact force, such as the rolling friction force of the road surface toward the tires, can be ignored. The velocity of vehicle v (at moment 0) before the collision occurs decreases to 0 and then increases to -v′ (moment t′). The impact that the rigid barrier exerts on the vehicle can be expressed with impulse P. Integrating for the duration of the impact, we can obtain the impulse that the rigid barrier exerts on the vehicle, which is calculated in the equation below:

$$P = \int_0^{t'} F(t)dt = \int_0^{t'} madt = m(v' - v) = m\Delta v. \tag{1}$$

As shown in Eq (1), impulse is equal to the change in momentum, and velocity difference Δv can represent impulse. The ratio of the vehicle speed after the vehicle impacts the rigid barrier and enters the rebound stage to the speed before the collision is expressed with the coefficient of restitution [15]. Coefficient of restitution e refers to the ratio of the impulse that the vehicle received in the rebound process to the impulse that the vehicle received in the compression deformation process. It can be expressed with velocity in the equation below:

$$e = -\frac{v'}{v}. \tag{2}$$

The collision between objects is an elastic collision (or completely elastic collision) when e = 1, an inelastic collision when 0 < e < 1 or a completely inelastic collision when e = 0, as the object does not rebound at all after collision. Finding solutions repetitively after changing the velocity parameters in the simulation model, the relationship between vehicle rebound speed and restitution coefficient as shown in Figure 7 can be obtained, the unary quadratic fitting curve of e is e = 62.42-1.89v + 0.0196v^2. Fitting R^2 is 0.983 (valid), but it is not an exactly quadratic relationship. Because the higher the collision speed is, the lower the restitution coefficient is, there is no inflection point till it becomes 0, when the collision speed is 50 km/h, and the value of the restitution coefficient is about 15%.

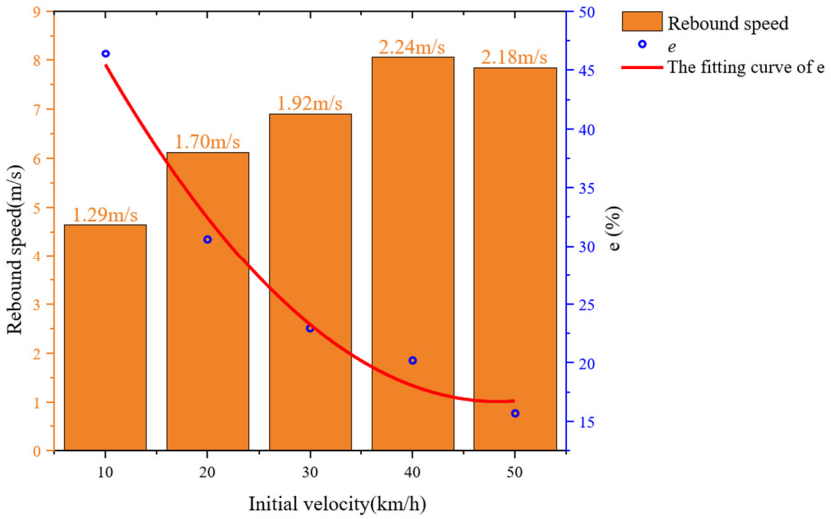

Figure 7. Rebound velocity and restitution coefficient.

After the vehicle crash occurs, high speed or low speed, there are always two energy absorptions in every part: plastic energy absorption (Ed) and elastic energy absorption (Ep). The maximum deformation energy is equal to the sum of the two. Once the crash occurs, automobile parts immediately start deforming, but they will partly rebound after the crash ends, and the displacement of the rebound will decrease as the vehicle collision speed increases. The parts on the vehicle feature less elastic energy absorption but more plastic energy absorption. As the vehicle deforms, the kinetic energy of the vehicle gradually converts into the deformation energy of the vehicle body. When the vehicle speed declines to 0, deformation energy reaches its maximum value. Then, the vehicle starts to rebound and eventually completely get away from the rigid barrier at velocity v′. While at low speed, the collision can be regarded as an elastic collision, but once the collision exceeds a certain threshold value, it will be regarded as a non-elastic collision. The moment, the vehicle body has residual deformation (namely permanent deformation), and causes energy loss (the lost energy is represented by E_D). The deformation amount of the vehicle body at this moment is different from the maximum deformation amount, and it is called the residual deformation amount.

When the vehicle collides with the rigid barrier, the maximum deformation energy E is equal to the initial value of vehicle kinetic energy $mv^2/2$. The lost energy E_{D} can be calculated in the equation below according to the kinetic energy before and after the collision:

$$E_{\mathrm{D}} = \frac{1}{2}mv^2 - \frac{1}{2}mv'^2 = \frac{1}{2}mv^2(1-e^2) = E(1-e^2) \tag{3}$$

As shown in Eq (3) above, when the coefficient of restitution e is 0, E_{D} is equal to E. When the collision speed is 50 km/h, the coefficient of restitution e is about 15%. As the coefficient of restitution decreases, the lost energy will increase.

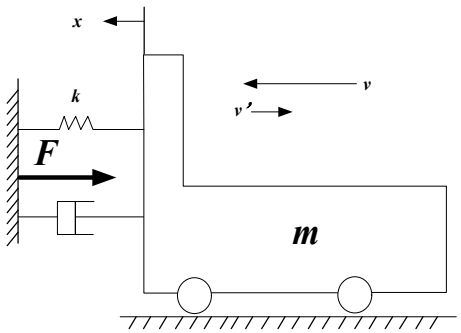

Figure 8. Spring-Mass Model for the collision of vehicles with rigid barrier.

When analyzing vehicle collision from the perspective of momentum and impulse, the time sequence changes of vehicle motion during the collision cannot be known. Therefore, we can simplify the collision of a vehicle with rigid barrier as the transient response problem of a spring-mass system, as shown in Figure 8, to analyze the motion of the vehicle when impact is exerted on the vehicle body. Suppose the elastic coefficient (namely, body stiffness) is k when the vehicle is loaded (compressed) and k' when it is unloaded (rebounds).

3.2. Course inversion

Under initial condition: At moment 0, suppose the speed of mass point (vehicle) is v, and displacement is 0. Suppose the length of the spring at moment 0 is its natural length, and the motion equations of the spring (vehicle body) during compression and rebound are

$$\begin{cases} m\ddot{x} = -kx & \text{(while in loaded state)} \\ m\ddot{x} = -k'(x - C) & \text{(while in unloaded state)} \end{cases} \tag{4}$$

where C represents residual deformation amount, according to the law of conservation of mechanical energy. The elastic coefficient can be expressed using collision speed v and maximum deformation amount *x*_max in the equation below:

$$k = \frac{mv^2}{x_{\max}^2}. \tag{5}$$

Take the initial conditions into Eq (4), a symbol equation w = √(k/m), w^' = √(k^'/m) which is similar to fixed frequency is obtained. Vehicle acceleration, velocity and displacement are shown in Eqs (6) and (7). At the point where the vehicle changes from the loaded state into the unloaded state, the change of vehicle displacement and velocity is continuous, and so is the change of vehicle acceleration.

1) While in loaded state ($0 \le t \le \pi/(2w)$)

$$\begin{cases} \ddot{x} = -vwsinwt \\ \dot{x} = vcoswt \\ x = \frac{v}{w}sinwt \end{cases} \tag{6}$$

2) While in unloaded state ($\pi/(2w) \le t \le \pi/(2w) + \pi/(2w')$)

$$\begin{cases} \ddot{x} = -vwcosw'(t - \frac{\pi}{2w}) \\ \dot{x} = -\frac{vw}{w'}sinw'(t - \frac{\pi}{2w}) \\ x = \frac{vw}{w'^2}\left\{cosw'\left(t - \frac{\pi}{2w}\right) - 1\right\} + \frac{v}{w} \end{cases} \tag{7}$$

As the maximum deformation $x_{\max} = v/w'$, take $t = \pi/(2w) + \pi/(2w')$ in formula 3 of Eq (7), and the residual deformation amount $C = v(1/w - w/w'^2)$ can be worked out. In addition, when $t = \pi/(2w) + \pi/(2w')$, the velocity of the vehicle when it leaves the rigid barrier $v' = -vw/w'$ can be obtained using formula 2 of Eq (7), Therefore, the coefficient of restitution e can be expressed with the elasticity coefficient of the spring in the equation below:

$$e = -\frac{v'}{v} = -\frac{1}{v}\left(-\frac{vw}{w'}\right) = \frac{w}{w'} = \sqrt{\frac{k}{k'}}. \tag{8}$$

The impulse that the rigid barrier exerts on the vehicle is calculated using Eq (9). Its final result is consistent with that of Eq (1), which also reflects the rationality of the equation.

$$\begin{aligned} P &= \int_0^{\pi/2w+\pi/2w'} Fdt = \int_0^{\pi/2w+\pi/2w'} m\ddot{x}dt \\ &= \int_0^{\pi/2w}(-mvw)sinw + \int_{\pi/2w}^{\pi/2w+\pi/2w'}(-mvw)cosw'\left(t - \frac{\pi}{2w}\right)dt \\ &= [mvcoswt]_0^{\pi/2w} - \left[\frac{mvw}{w'}sinw'\left(t - \frac{\pi}{2w}\right)\right]_{\pi/2w}^{\pi/2w+\pi/2w'} \\ &= -mv - \frac{mvw}{w'} = m(v' - v) \end{aligned} \tag{9}$$

3.3. Examples of vehicle front crash inversion

In this section we will apply the spring-mass model in the 100% overlap rigid barrier collision test analysis for a passenger vehicle. Given the mass of the vehicle m = 1500 kg, collision speed v = 50 km/h (13.89 m/s), the maximum deformation amount after the crash is measured to be x_max = 0.636 mm, and according to the vehicle speed sensor inside the vehicle, the rebound velocity measured is v′ = 2.18 m/s.

First of all, obtain the expression $w = v/x_{\max} = 13.89/0.636 = 21.84$ rad/s, which is similar to intrinsic frequency, namely, $t = 0.072$ s at $t = \pi/(2w)$, when the vehicle deformation reaches the maximum value using formula 6 of Eq (6). Next, obtain w' = -139.15 rad/s based on v, v', w using Eq (8). Take in the data, and obtain the vehicle velocity, displacement and time change curves using Eqs (6) and (7). The result of the comparison between the data of the inversion equation and simulation test shows that, the two are nearly the same as each other in the change tendency of velocity, displacement and time in vehicle collision. As shown in Figure 9, as the collision goes ahead, the velocity of the vehicle gets slower and slower, and the vehicle front starts to absorb energy, converting kinetic energy into internal energy. The velocity decreases to 0 at 72 ms, when it releases internal energy and rebounds.

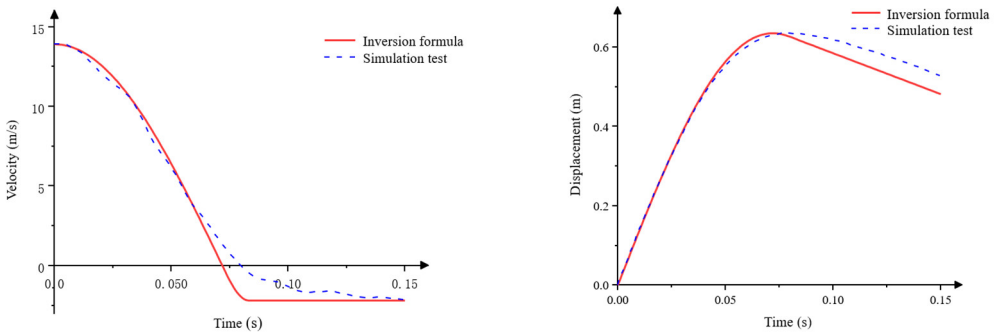

Figure 9. Calculation results for 100% overlap rigid barrier collision course simulation.

As shown in Eq (10), error determination coefficient R^2 is used to perform error analysis over inversion model and simulation test. The closer its value is to 1, the better the correlation between actual and predicted values. Since the inversion rate of vehicle speed is 98.35%, and the inversion rate of displacement is 97.47%, it indicates that the inversion is effective.

$$R^2 = 1 - \frac{\sum_{i=1}^{N}(y_i - \hat{y}_i)^2}{\sum_{i=1}^{N}(y_i - \overline{y})^2} \tag{10}$$

where y_i and $\hat{y}_i$ represent the true and predicted values, respectively, $\overline{y}$ is the average of the true values, and N is the number of samples.

As the momentum obtained using the two groups of course inversion equations, i.e., Eqs (6) and (7), meets the law of conservation of momentum, this proves the scientificalness of the inversion equation from the perspective of momentum conservation. That is to say, through the rebound velocity and the maximum deformation of the vehicle after the front crash, we can invert the velocity and displacement curves of the entire collision course of the vehicle.

3.4. Examples of front bumper drop weight inversion

The inversion research of the vehicle also provides a theoretical basis for the inversion of the front bumper. Next, we present the research on the collision course inversion of the bumper on the basis of the inversion algorithm derived from vehicle crash.

Given the mass of the drop weight m = 1500 kg, collision speed v = 4 km/h (1.11 m/s), the maximum deformation amount after the crash is measured to be $x_{\max}$ = 11.6 mm, and rebound velocity measured using the drop-weight sensor is v' = 0.387 m/s.

First of all, work out the expression similar to fixed frequency $w = v/x_{\max} = 1.11/11.6 \times 10^{-3} = 95.69$ rad/s, namely, $t = 0.016$ s, at the moment $t = \pi/(2w)$ when vehicle deformation is maximum, using formula 3 of Eq (6).

Next, take into account of the impact of gravity and conduct rewriting according to Eq (8) and dynamics principles.

1) While in loaded state ($0 \le t \le \pi/(2w)$)

$$\begin{cases} \ddot{x} = -vwsinwt + g \\ \dot{x} = vcoswt + gt \\ x = \frac{v}{w}sinwt + \frac{1}{2}gt^2 \end{cases} \tag{11}$$

2) While in unloaded state ($\pi/(2w) \le t \le \pi/(2w) + \pi/(2w^{'})$)

$$\begin{cases} \ddot{x} = -vwcosw'(t - \dfrac{\pi}{2w}) + g \\ \dot{x} = -\dfrac{vw}{w'} sinw'(t - \dfrac{\pi}{2w}) + gt \\ x = \dfrac{vw}{w'^2}\left\{cosw'\left(t - \dfrac{\pi}{2w}\right) - 1\right\} + \dfrac{v}{w} + \dfrac{1}{2}gt^2 \end{cases} \tag{12}$$

Using Eq (8), work out w' = -274.707 rad/s based on v, v', w. Figure 12 shows the vehicle acceleration and speed obtained using Eqs (11) and (12). According to Figure 10, the bumper is stricken again due to the impact of gravity incurred by the drop weight. For this reason, the calculation of drop weight inversion is limited to the process before the secondary collision, while the comparison result of the figure shows the inversion effect of speed and deformation amount is good. Comparing and analyzing the simulation test and inversion formula data analysis, the time-velocity and time-deformation curves of the two are basically the same. Although there are certain differences between the inversion prediction and the simulation data results, the overall accuracy can be guaranteed. The collision course can be quickly deduced by using the inversion formula. The inversion research can effectively improve the efficiency of solving the collision course while ensuring the accuracy.

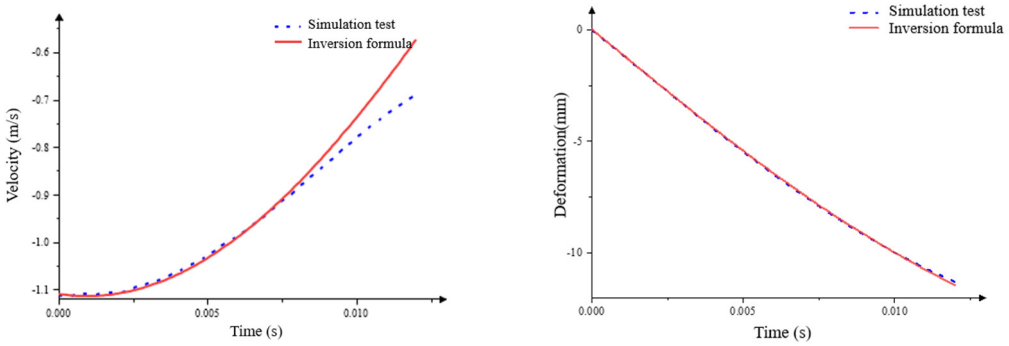

Figure 10. Inversion course computation result of bumper.

4. Analysis of front bumper

4.1. Theoretical analysis

To study the deformation form energy-absorption behavior of the bumper, first of all, we need to determine the boundary conditions of the collision. Figure 11 shows the energy-absorption data of each part in the vehicle simulation. Observation finds that entire bumper system can keep a minimum 40% energy absorption if vehicle speed is lower than 40 km/h. If the speed is higher than 40 km/h, as front longitudinal beam and A-pillar join in the energy-absorption, the energy-absorption contribution of the front bumper will decrease. The energy-absorption contribution reaches the highest value 64% at a speed of 20 km/h. The front crash tests over vehicle energy levels (pendulum collision, sled collision, vehicle collision) made the following conclusion:

While in the crashworthiness test for the front bumper, the velocity should approach 20 km/h

to the most possible extent. Objectively, this is also AZT-Crash-Reparatur-Test (Germany), the test of RCAR, because under low-speed bumper regulation and standard, only the two approached 20 km/h. The test speed will approach 20 km/h to the most possible extent in the bumper crash test and analysis in the section below.

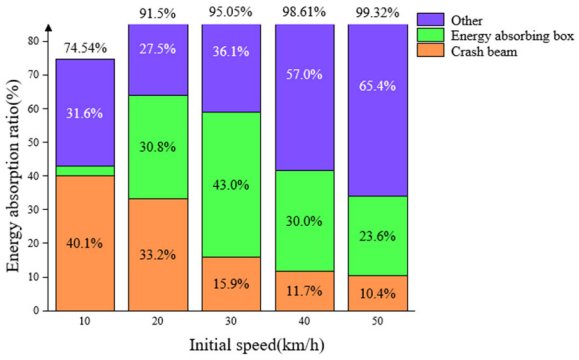

Figure 11. Energy-absorption contribution of each part at different speeds.

Illustrate a group of cylindrical hammer drop isoenergetic simulation, in all of which, drop energy is 350 kJ, v_1 = 26.45 m/s for high speed v_2 = 7 m/s for low speed. The masses of drop weight controlled under this energy were 14.3 and 1 kg, respectively. Figure 12 shows the simulated kinetic energy dissipation image. It indicates the initial kinetic energy is the same, and the kinetic energy dissipation varies at different collision speeds v_1, v_2 ($v_1 > v_2$). Even in the end state, high speed dissipates a little more kinetic energy than low speed.

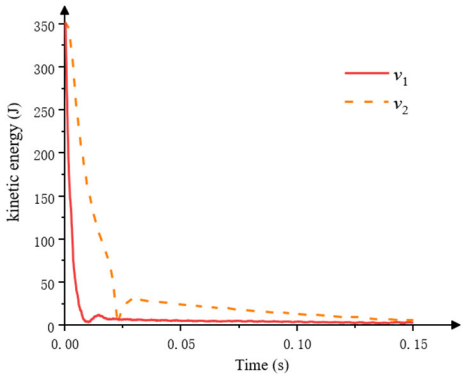

Figure 12. Kinetic energy dissipation diagram of bumper crash drop weight test.

Figures 13 and 14 show the comparisons between the stress nephograms and final position displacement nephograms of low-speed collision and high-speed collision. According to the figures, the stress of low-speed collision is lower, at 755.6 MPa; while the stress of the high-speed collision is higher, at 778.9 MPa. By contrast, the final displacement value of low-speed collision is higher, at 97.3 mm, while the displacement value of high-speed collision is lower, which at 76.5 mm. From the figures, we obviously see, in high-speed collision, the surrounding radiation circle of the stress is very large, and so is the position displacement nephogram of high-speed collision. The deformation has a tendency to extend toward both ends.

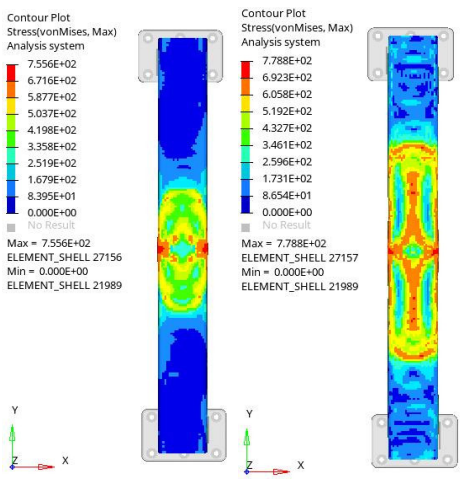

Figure 13. Comparison of stress nephograms between low-speed collision (left) and high-speed collision (right).

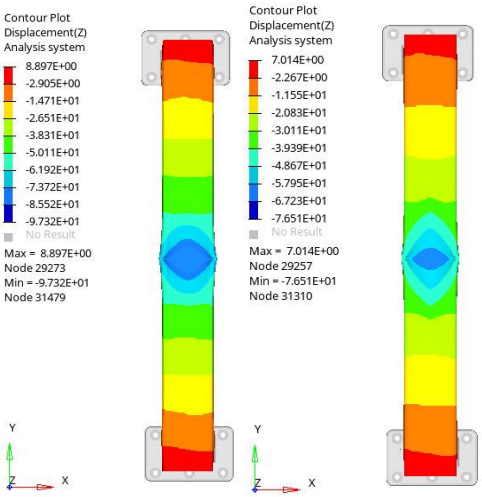

Figure 14. Comparison of final displacement nephograms between low-speed collision (left) and high-speed collision (right).

To sum up, as shown in Figure 15, the speed at collision contact center will be higher than that in the area around it, so at constant energy, comparison between low-speed collision and high-speed collision shows, the deceleration in the surrounding area of high-speed collision is lower, while the deceleration in the surrounding area of low-speed collision is higher. Accordingly, the distance of radiation outward from center varies, and the deformation radiation distance of high-speed collision is longer, while the deformation radiation distance of low-speed collision is shorter. In addition, this phenomenon has similarities with heavy objects falling in water.

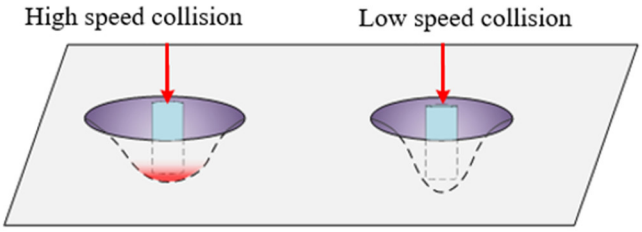

Figure 15. Plane collision deformation radiation distance.

4.2. Test validation

The original weight of the drop weight was 14.3 kg, and each square counterweight is about 3.14 kg. The total mass m of the drop weight can be weighed using a hook scale. Perform constant-energy test based on the equation E = mgh, h_2 = m_1 h_1/m_2， v = [(2gh)]^(1/2), g = 9.8 m/s^2. The height of the drop weight is determined using the ruler on the side, and the height of the drop weight is adjusted to be initial height plus h. The final intrusion Δd is measured using the Laser Rangefinder described above. Read the data d_1 before dropping the weight, read d_2 after dropping the weight, and Δd = d_2-d_1. According to the conclusion drawn above, for bumper crashworthiness test, the velocity should approach 20 km/h to the most possible extent. See Table 2 for the variables of the test.

Table 2. Variables of drop weight test.

No.	m (kg)	h (m)	E (J)	v (km/h)
1	14.3	2.500	350.35	25.2
2	16.8	1.128	350.354	23.2
3	19.2	1.862	350.354	21.75

Figure 16 shows the acceleration images acquisitioned in three tests. According to the image, although the acceleration fluctuates widely, it has two peak values. One is generated when hammer collides with anti-collision beam, it compressed to a maximum value of collision force; the other is generated when anti-collision beam contacts the protective underlay, as the compression amount generated the moment is very small, the collision force will rise dramatically.

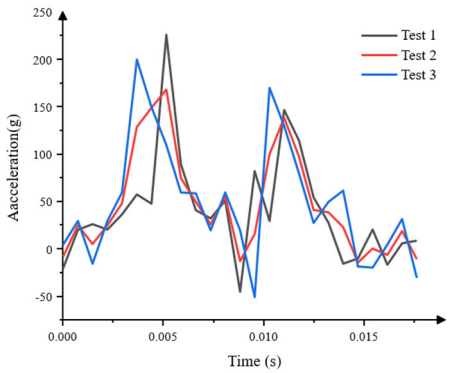

Figure 16. Acceleration acquisition image.

Figure 17 shows the real photos taken before and after bumper crash. It obviously indicates that, test 1 is a relatively low-speed test, and the deformation radiation distance is shorter. Meanwhile, test 3 is a relatively high-speed test, the deformation radiation distance is longer.

Figure 17. Bumper crash deformation analysis.

Finally, according to the test data recorded in Table 3, the final intrusion of test 3 is higher than that of test 1, and this proves the theoretical analysis that low-speed deformation is greater than high-speed deformation.

Table 3. The records of final intrusion results.

No.	E (J)	V (km/h)	d1 (m)	d2 (m)	Δd (m)
1	350.35	25.2	1.229	1.3	0.071
2	350.354	23.256	1.229	1.297	0.068
3	350.354	21.744	1.229	1.295	0.066

5. Conclusions

1) A crash inversion prediction method is proposed, and a simulation model and spring-mass model are used to conduct inversion study on vehicle crash and automobile front bumper crash. The changing tendency of the time-velocity curve and the time-deformation curve obtained by the collision inversion algorithm are basically consistent with the simulation test results. The inversion rate of vehicle frontal collision speed is 98.35%, and the inversion rate of displacement is 97.47%, indicating that inversion algorithm can quickly derive collision course, and it can be used to replace some test or finite element simulation in practical applications, effectively improve the efficiency of solving collision course.

2) Solution to repeat by changing the speed of the vehicle simulation model parameters, the function relationship between vehicle speed and collision recovery rate for e = 62.42-1.89v + 0.0196v^2. In other words, within a certain range, the higher the collision speed is, the lower the restitution coefficient is.

3) Take the vehicle speed boundary conditions in the test to conduct validation, and the relationship between low-speed collision and high-speed collision of front bumper is obtained. The comparison of high-speed collision and low-speed collision of the same energy shows that, the deformation radiation distance of high-speed collision is longer, while the deformation radiation distance of low-speed collision is shorter, and in front bumper crash, the deformation depth of low-speed collision is greater than that of high-speed collision.

Acknowledgments

This work is supported by the research fund of the National Natural Science Foundation of China (Grant No. 52175239) and by the Shanghai Automotive Industry Technology Development Foundation (Grant No.1744).

Conflict of interest

The authors declare that there is no conflict of interest.

References

1. G. Tang, J. Liu, Z. She, J. Li, Analysis and optimization on front bumper crash structural performance of a blade electric vehicle, *Automob. Technol.*, **47** (2022), 64–67. https://doi.org/10.16638/j.cnki.1671-7988.2022.007.013
2. S. Wang, P. Xu, D. Wang, W. Guo, Q. Che, Inversion prediction method of subway composite energy absorption structure parameters, *J. Railway Sci. Eng.*, **19** (2022), 3087–3095. https://doi.org/10.19713/j.cnki.43-1423/u.T20211358
3. L. Zhang, X. Zhao, L. Gan, H. Li, Y. Zheng, C. Zhou, Finite element simulation of ship collision accident inversion, *Navig. China*, **41** (2018), 78–83.
4. M. Duan, Study on ship bridge collision test based on ship equivalent model, *J. Chongqing Jiaotong Univ.*, 2017.
5. Y. Liu, *Research on Ice Load Inversion Method and Application of Polar Sailing Ships*, M.A thesis, Harbin Engineering University, 2017.
6. L. Han, *The Research on Inversion Problems in Sheet Metal Forming Processes Based on Neural Network*, M.A thesis, Hunan University, 2006.
7. S. Yang, *A Inversion Method of Material Parameters about the CFRP Used in Vehicles*, M.A thesis, Hunan University, 2015.
8. J. Yang, H. Xu, J. Zhao, J. Lei, Research on composite control of lateral position of lane line based on inversion and sliding mode, *J. Highway Transp. Res. Dev.*, **32** (2015), 153–158.
9. G. E. Backus, J. F. Gilbert, Numerical applications of a formalism for geophysical inverse problems, *Geophys. J. Int.*, **13** (1967), 247–276. https://doi.org/10.1111/j.1365-246X.1967.tb02159.x
10. G. E. Backus, J. F. Gilbert, The resolving power of gross earth data, *Geophys. J. Int.*, **16** (1968), 169–205. https://doi.org/10.1111/j.1365-246X.1968.tb00216.x
11. G. E. Backus, J. F. Gilbert, Uniqueness in the inversion of inaccurate gross earth data, *R. Soc.*, **266** (1970), 123–192. https://doi.org/10.1098/rsta.1970.0005
12. H. Gao, *Research on Key Technologies of Vehicle Contact Collision Simulation*, Ph.D thesis, Hunan University, 2008.
13. M. Huang, *Vehicle Crash Mechanics*, New York, CRA Press, (2002), 69–138. https://doi.org/10.1201/9781420041866
14. S. Qiu, *Vehicle Collision Safety Engineering*, Beijing Institute of Technology Press, 2016.

15. X. Wang, W. Lin, G. Liu, S. Ma, R. Tong, Research progress of impact force based on Newton's impact recovery coefficient evaluation, *Mech. Sci. Technol. Aerosp. Eng.*, **39** (2020), 1526–1533. https://doi.org/10.13433/j.cnki.1003-8728.20200179